Optical metrology for the segmented optics on the Constellation-X Soft X-ray telescope

David Content[a], David Colella[b], Charles Fleetwood[c], Theo Hadjimichael[c],
Timo Saha[a], Geraldine Wright[a], William Zhang[a]
[a]NASA Goddard Space Flight Center, Greenbelt MD 20771; [b] Mantech, Inc, NASA GSFC, MC540.5, Greenbelt, MD 20771; [c]Swales Aerospace, 5050 Powder Mill Rd, Beltsville, MD

ABSTRACT

We present the metrology requirements and metrology implementation necessary to prove out the mirror technology for the Constellation-X (C-X) soft x-ray telescope (SXT). This segmented, 1.6m diameter highly nested Wolter-1 telescope presents many metrology and alignment challenges.

A variety of contact and non-contact optical shape measurement, profiling and interferometric methods are combined to test the forming mandrels, some of the replication mandrels, the formed glass substrates before replication and the replicated mirror segments. The mirror segments are tested both stand-alone and in-situ in mirror assemblies. Some of these methods have not been used on prior x-ray telescopes and some are feasible only because of the segmented approach used on the SXT.

Methods to be discussed include axial interferometric profiling, azimuthal circularity profiling, midfrequency error profiling, and axial roughness profiling. The most critical measurement is axial profiling, and we compare the method in use to previous methods such as the long trace profilometer (LTP).

A companion paper discusses the method of non-contact 3D profiling using a laser sensor and distance measuring interferometers.

Keywords: Optical Metrology, x-ray optics, Constellation-X

1. INTRODUCTION

This paper will present the requirements, methods, and initial results for the optics being fabricated and assembled for the technology development program on the Constellation-X (C-X) soft x-ray telescope (SXT). This is a summary of work in progress. After a brief introduction to the telescope design, the mirror segment design and fabrication and alignment flow are described to lay out the metrology challenges. Each portion of the metrology is described and examples and analysis given.

The Constellation-X follow-on mission now under development [1] aims to collect many more x-ray photons from each source (as compared to current missions including Chandra, XMM, and Astro-E2) so as to allow x-ray spectroscopy on many more sources. Our aim is a highly sensitive soft x-ray space observatory (0.25-10 keV energy, or ~6 to 0.1 nm wavelength range) [2]. Each of 4 identical co-pointed telescopes will be comprised of many (~170-230 depending on the eventual choice of an axial length) [3] nested thin (~0.4 mm) shells of grazing incidence mirrors. The work is collaboration between GSFC, MIT, MSFC, and SAO developing the technologies required to fabricate, assemble, align, and test these telescopes. Other papers in this session cover aspects of the design [3], systems analysis & error budgeting [4], fabrication [5-6], alignment [7], and x-ray testing [8] of these optics. A companion paper to this one [9] details efforts to develop 3-D shape measurements of the individual optic segments using non-contact profilometry (see also [10]).

As compared to conventional optics (e.g. those used in ground based normal incidence instruments), these are unusual optics. As one example, a rule of thumb for a conventional mirror, to be sufficiently stiff under gravity loading, is for the diagonal to thickness ratio (aspect ratio) to be ~6:1. As detailed in table 1, the current optics are 800:1 and eventually the flight mirrors may be significantly more extreme. Thus these are by any normal consideration, flimsy optics.

The prescription for these mirrors is either segments of a Wolter-1 [11] primary or secondary, or, nearly equivalently [3], segments of 'equal curvature' telescopes consisting of axially sagged conical mirrors. In either case the desired axial sag from the base cone shape is a few microns or less. Each mirror is ~0.4mm thick, made from a glass substrate [5-6] formed over a convex forming mandrel and then epoxy replicated over a superpolished replication mandrel. The areal density of a single segment is then ~1 kg/m^2. These optics can be described as ultralightweight, extreme off-axis segmented aspheres.

The implication is that all operations on these optics, specifically including all metrology and alignment, must be made with great care. The question as to whether we can in practice mount these optics without any significant stress in the lab or in a flight-like housing is still open. Gravity distortions can be significant as well, depending on orientation.

We are building several test assemblies; the sequence is as follows: Currently we are using an 8.4m focal length, electroless Ni replication mandrel with ~245mm radius (and primary and secondary sections). The Optical Assembly Pathfinder (OAP) will use this mandrel and various iterations of housings to prove out the process. We expect to follow this with a flight-design outer module pair (sparsely filled with high-quality optics), called the prototype. The current design for flight (30cm axial length case) is also shown in Table 1 for comparison.

					C-X SXT assemblies		
	units	AstroE2	Chandra	XMM	OAP	Prototype	Full flight (30cm)
Largest mirror radius	mm	106	600	350	247.5	800	800
angular width	degree	90	360	360	56	30	30
arc length	mm	167	n/a	n/a	241.9	418.9	418.9
axial length, per reflection	mm	100	420	300	200	200-300	300
part diagonal	mm	194	n/a	n/a	314	464-515	515
substrate thickness	mm	0.155	30	0.85	0.4	0.4	0.4?
aspect ratio		1253	14	353	785	1160-1288	1288?

Table 1: Mirror aspect ratio comparison for various missions and stages of the C-X SXT development. For full shells, the aspect ratio is simply the length over the thickness (average of extreme values when varying with shell number); for the segmented telescopes it is the reflector segment diagonal over the thickness.

Table 2 compares the individual mirrors for C-X SXT, Chandra, XMM, and AstroE2 as well as respective angular resolution requirements (half-power diameter or HPD in arcseconds). A metric expressing the relative difficulty would be the product of the HPD to the segment areal density (as each being lower allows more science for a given launch weight). The metric for C-X is significantly lower than all of the others, suggesting the challenge in measuring these optics is more extreme. Also, the HPD goal of 5 arcsec for the SXT will push these issues even harder.

mission	mirror material	density	thickness	areal density	Required HPD	product HPD *areal density
units		kg/m^2	mm	kg/m^2	arcsec	arcsec* kg/m^2
AstroE2	Al	2700	0.2	0.42	90	38
Chandra	Zerodur	2530	30.0	75.90	0.5	38
C-X SXT	Desag 263	2510	0.4	1.03	15	15
ROSAT	Zerodur	2530	20.0	50.60	3	152
XMM	Ni	8908	0.9	7.57	15	114

Table 2: Comparison of required half-power diameters, areal densities, and product for various missions. As both areal density and HPD are ideally small, their product is in some sense a metric of the difficulty of the mirrors.

To understand the metrology required, the fabrication and alignment sequence is summarized (for more details see Refs 4-7). After all necessary metrology on mandrels is performed, the steps (in brief, see Ref [7] for details) are:

1. Thin sheets of D-263 are formed over a convex forming mandrel at ~600° C into mirror substrates.
2. Metrology (typically axial profiles (§3.3), roughness (§3.6), and perhaps circumferential profiles (§3.2)) is performed.
3. Selected substrates are spray coated with a thin epoxy layer and replicated using a precision replication mandrel.
4. The metrology from step 2 is repeated.

5. Selected replicas are installed into test housings and top and bottom adjusters at 5 azimuthal positions are installed and located at the correct radius.
6. "In-situ" circumferential profiles near the axial positions of the adjusters are measured to ensure no distortion from small (~2um) positional errors.
7. A combination of repeat, in-situ axial interferometry and grazing incidence slope measurements, using the centroid detector assembly (CDA) [12] and adjustments to the actuators to correct slope and radius errors, is used to align first a primary (P) segment and then combinations of primary and secondary (S) segments.
8. The aligned mirror(s) are epoxy bonded into place; the P and S modules are aligned and bonded together; metrology is repeated as necessary and the assembly is ready for x-ray testing.

Optical metrology is then essential feedback to each of the fabrication, alignment, and assembly steps.

2. METROLOGY REQUIREMENTS

The requirements for the metrology flow from the manufacturing and alignment sequence above and from the nature and precedence of the error contributions to the overall x-ray imaging performance. We have developed and maintained an error budget for the initial x-ray testable mirror assemblies and for the flight mirror. If one imposes on each term the requirement that metrology errors are only 10% of the relevant term in the error budget, in a root-sum-squared sense, then the implication is that each measurement must be ~ 1/3 =1/sqrt(10) of the relevant mirror error allocation.

Table 3: Metrology matrix		**Requirement**		**Mandrel metrology**		**Substrate/Replica metrology**		**note**
Error term	**units**	**Part**	**Metrology**	**perfor-mance**	**method**	**perfor-mance**	**method**	
Average radius error	um	10	3.2	±2	CMM	tbd	nC CMM	
Cone angle deviation	arcsec	10	3.2	±5		tbd		
Delta-delta-r error, rms	arcsec	0.6	0.2	0.6		0.1	CDA	1
Roundness (in phase) or azimuthal figure, rms	um	4	1.3	0.3		(1)	nC CMM	
Axial sag error	um/m^2	40	14	±1	Wyko400/ 8BX	(±1)	Wyko400/ 8BX	2
Axial slope irregularity, rms	arcsec	1	0.3	0.35		0.5		
Midfrequency error, rms	nm	1.3	0.4	0.1	Bauer200	(0.1)	Bauer200	2
Microroughness, rms	nm	0.3	0.1	0.1	MicroXAM	0.1	MicroXAM	
notes								
1. CDA applicable to P or S substrate or replica in a housing or assembly								
2. Parentheses indicate the expected value, but confirmation is incomplete on this type of part								

Table 3: Metrology requirements for mandrels, and (substrates and replicas) as a function of spatial frequency. Equipment, data examples, calibration, and uncertainties are discussed in more detail below.

To simplify this discussion, we do not break down the errors in to a full set (e.g. distinguishing in-phase out of roundness ("delta-R") from out-of-phase ("delta-delta-R") etc.) but rather classify them according to spatial frequency. The overall error budget itself is more thoroughly discussed elsewhere, e.g. [4]. The metrology requirements that result from this analysis are summarized, along with the spatial frequency range and equipment used, in Table 3.

The requirement for each term by part is listed, along with the metrology requirement. The methods and current performance for mandrels on the one hand and the substrates & replicas on the other hand are listed on the right side.

This table is in preliminary form. For example, it may in the future arise that we need better metrology for a particular term on the mandrels than on the substrates, or on the replicas than the substrates. We do see in practice that, as the substrates currently have significant mid-frequency type errors, interferometry on them is more difficult (high local slopes can be difficult to resolve).

Generally speaking the mandrel metrology is shown to be well in hand, with the possible exception of the delta-delta-R error. As this error in the final instrument is strongly controlled by the alignment process, it isn't clear that better metrology on the mandrels is essential. The metrology on the substrates and replicas is not as far along, with the axial slope irregularity not quite being repeatable and accurate enough yet. Note that some qualifying measurements are shown that are taken using metrology applicable to substrates (e.g the non-contact probe) but the measurements were performed on mandrels so that the traditional contact probe could also be used to check accuracy.

3. METROLOGY IMPLEMENTATION

3.1 Lowest order – shape metrology

The cone angle and radius ideally are measured not only for the mandrels, but also on the formed substrates (with comparison to the values for the section of the mandrel used for forming) and on the replicated mirror segment. We separate mandrel measurements from measurements on substrates and mirrors because different methods are in use for the two cases, because of the inability to measure the very thin substrates and mirrors using a standard contact probe. We hope in future to combine all measurement setups into one using a single non-contact (optical) probe.

Both types of metrology, however, are in general implemented on a Moore#3 coordinate measuring machine (CMM) [9,10] which has a ~45 cm maximum travel in its longest axis. Motion in each axis is monitored by distance measuring interferometers and can be logged on a computer. We currently have three probe types; a standard contact probe (6g contact force), a low-force probe (14 mg contact force), and an optical probe [13]. The CMM is in a lab with decent (e.g. typically ±2°C) temperature control. This machine, while the highest precision CMM available on the program, is undersized for the 50cm mandrel diameters and so significant work-around is required for some of the measurements described here.

3.1.1 Moore CMM contact probe measurements on mandrels

The diameter and cone angle must be checked for each mandrel, as significant errors in these basic dimensions will be carried through the optical fabrication flow but can not be overcome by any alignment or mounting scheme, and so will cause unacceptable image errors. The contact measurements are made at 4 azimuthal positions on the mandrel, which in many cases can not be certified to have its axis perpendicular to the base. This "out of squareness" significantly complicates the measurement, as there is no assurance that the direct measurements of the local slope corresponds to the actual cone angle. By averaging 4 azimuthal positions this out of squareness is compensated. The midpoint diameter is interpolated from two separate careful diameter measurements near the two ends of the part and a separate total axial length measurement.

Table 4 lists an example measurement, where we repeated the measurements to assess repeatability errors. The typical linear uncertainty in a single measurement is of order 1 micron; this is about what is required to meet the error budget.

Measured parameter	**Diameter**		**Cone Angle**	
F494S	**value**	**units**	**value**	**units**
specification	490.866	mm	1.2554	degree
specification tolerance	0.20	mm	30	arcsec
error from specification	0.16	mm	3.9	arcsec
metrology uncertainty requirement	0.070	mm	10	arcsec
metrology uncertainty	0.002	mm	9.2	arcsec

Table 4: Example shape data using contact CMM on a forming mandrel, including repeatability measurements.

3.1.2 Non-contact shape measurements on substrates & replicas

The non-contact measurements proceed rather differently, as the segments subtend no more than $1/6^{th}$ of a full shell and there is no intrinsic reference as to the orientation of the part. Our method (described more fully in the companion paper [9]) is to acquire 3-D profile data using the non-contact probe, and to interpret it as a partial map of (in general) a segment of a cone with 6 degrees of misalignment as well as radius and slope angle departures from the forming mandrel. This work is incomplete at this time, but we expect to use this approach as a major component of the metrology program to ascertain low order forming and replication shape errors.

3.2 Azimuthal error

Two general methods have been explored to acquire this information, which includes azimuthal error, roundness on mandrels, which in turn is sometimes decomposed into delta-r or 'in-phase' roundness error and delta-delta-r "out of phase" roundness error. The latter is much more significant as an aberration contributor, but can in some cases be mitigated by alignment freedoms available in the housing holding the mirror segment.

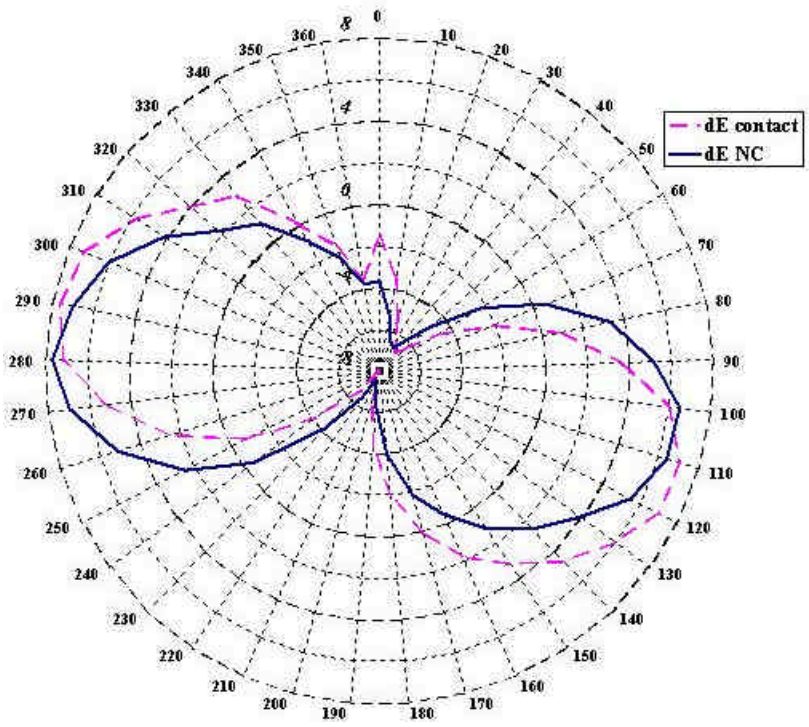

Fig. 1: Circularity error on a mandrel as measured using both a standard contact probe (dashed) and a non-contact optical probe (solid). The two methods both give good results and agreement between them is at the required level.

3.2.1 Interferometric profilometry for azimuthal error

We have attempted measurement of circumferential profiles using two approaches. The more precise is circular interferometry. It is the converse of the collimated beam interferometry described above; a narrow axial section of an (azimuthally concave) substrate or replica is returned to a spherical beam from a (fast, f/0.75 to overfill a 60° segment) transmission lens. This has typically not been successful, as the departure from circularity, at least as currently fixtured, exceeds the interferometer's dynamic range for wavefront error (typically about ~10 μm). As this error can be much larger than the axial figure error for the same increase in image size, this has not been of great concern.

This method is restricted to the (azimuthally concave) substrates and replicas, as fast (~f/0.75 to overfill a 60° segment) large transmission optics as would be required to work with our mandrels and compatible interferometers are not available (commercially or otherwise).

3.2.2 Contact profilometry for azimuthal profiles

A second method is to use the non- contact probe coupled with the CMM. As this measurement is still under development, at this time we can not say with certainty that it meets all requirements.

However, mandrels are sufficiently stiff as to measurable with the contact probe. Fig. 1 gives and example of a test taken on a mandrel with both of these probe types, showing the similarity in data (the standard deviation of the difference when small decentering misalignments, of order 5 microns or less, are removed, is ~2 μm). The overall shape measured and shown as delta-radius in the 'radar' type plot, is a slight oval-type out of roundness. This is not a concern, as the fabrication process uses only ~60° of the part and the radius variation is weak over this range. In each case the standard deviation of the out-of-roundness error is ~5 microns. Repeatability with the contact probe is at the full performance level of the CMM, which we have repeatedly found to be ~ 0.2 microns rms.

3.3 Axial profiles

The measurement of the axial profile is the most critical measurement we routinely make, and so bears a more extensive discussion. We present several potential means of measuring these profiles, including results of an experiment meant to check the accuracy of our chosen method. Also shown are results of repeat measurements.

This measurement is difficult as the optic is (ideally) a slight departure from a cone; the axial sag values for the optical prescription for the optics we currently have in the lab (for our optical assembly pathfinder or OAP) are < 2 microns. The cone angles are ~0.4° and ~1.2° for the primary and secondary optics, respectively, with radii in the range of 240-250mm, axial length of 20cm, and azimuthal extent of ~60°.

Early in this program we considered several alternate means of assessing axial figure. Initial schemes considered were cylindrical and conical wave interferometry, long trace profilometry, curvature measurement with integration, and collimated beam interferometry. To explain each of these in turn --

- Cylindrical wavefront interferometry uses a refractive or diffractive cylindrical null; these can be purchased, but not currently at the axial lengths we require (20-30cm). Instead, we have purchased the maximum size available, 8-9 cm both a cylindrical and conical computer generated hologram. The cylindrical null, used at a single azimuthal location, still provides a good wavefront match to a cone given optimal alignment. The conical null is the only approach which measures significant azimuthal and axial portions simultaneously; however we would need an inordinate number (currently 6-10, eventually ~500 or more) of these custom nulls and still they are nowhere near the axial extent required – the maximum available CGH diameter is 90mm standard and 150mm as a custom optic; we require at least 200mm and would prefer 300mm CGH sizes.

- The long trace profilometer [14] measures local slope; integration of this data provides a profile if drifts in the data can be avoided. This instrument is custom built to order, currently by Ocean Optics; our colleagues at the Marshall Space Flight Center use this method for the same application (e.g. [15]). We asked P. Takacs of Brookhaven, the developer of this instrument, to measure a mandrel as a test.

- We have a Bauer200 midfrequency measuring instrument [16]; this instrument measures local curvature, integration of which once (twice) provides local slope (profile) information, depending on drifts in the data. Unfortunately, drifts in this instrument remain at the level where it is difficult to measure low order errors, e.g. those with error periods > ~50 mm.

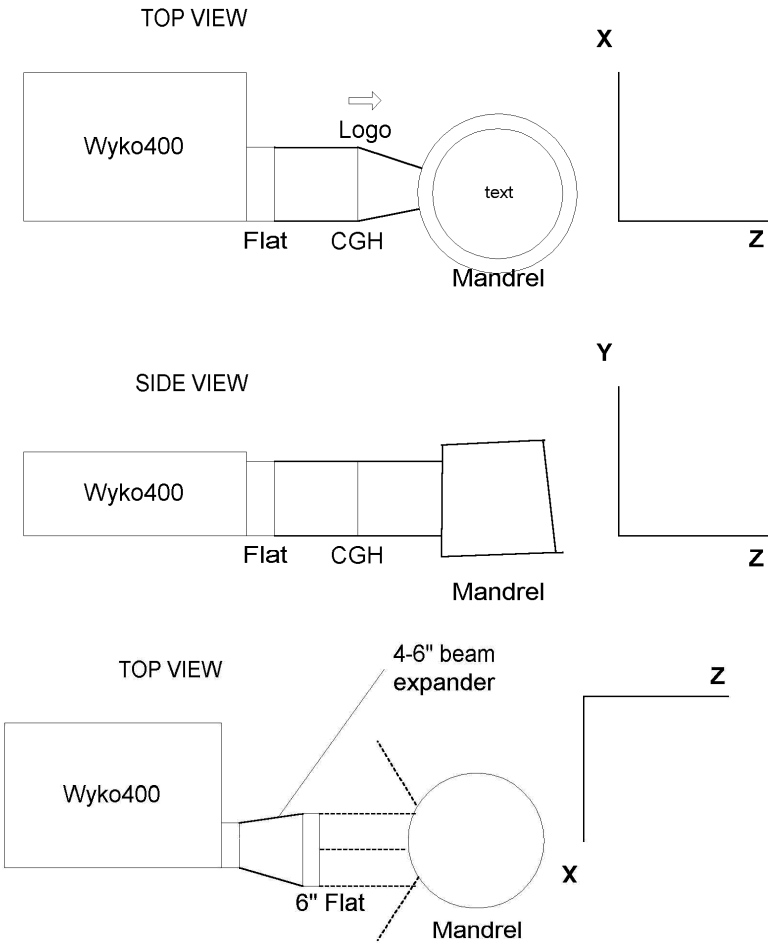

Fig. 2: Top: CGH –based test layout; Bottom: collimated beam interferometry layout.

- Collimated beam interferometry is simply measuring the axial figure departure from a plane wave over a very narrow azimuthal extent such that the portion measured

is essentially flat. The collimated beam can easily be calibrated and rechecked. Alignment is minimal – the relative tip of the part to the collimated beam must be adjusted, as opposed to the other methods, where typically tilt and/or focus must be adjusted as well.

None of these methods would easily apply to the full shell missions that have been used previously; while the alignment is much more complex, the segmentation allows a broader range of metrology measurements to be used in the mirror development.

Figure 2 shows the optical layout for the CGH-based and collimated beam interferometry approaches. Not shown are adjustments to the CGH necessary to allow repeat measurements and measurement overlap as necessary to allow stitching of the interferometry data. Our most critical axial figure measurements are made using the 20cm beam expander described below.

In either case, measurement of substrates and replicas is very similar, except that the azimuthally concave optic must be placed, in the case of CGH-based testing, at the far side of the azimuthal focus. Any optic can of course be in principle placed at any point along the collimated beam.

Figure 3 shows a comparison of axial figure and slope profiles from the Cylinder CGH, the LTP, and the collimated beam interferometry. The agreement to ~10 nm in axial figure provided the confidence that the collimated beam approach would meet our needs.

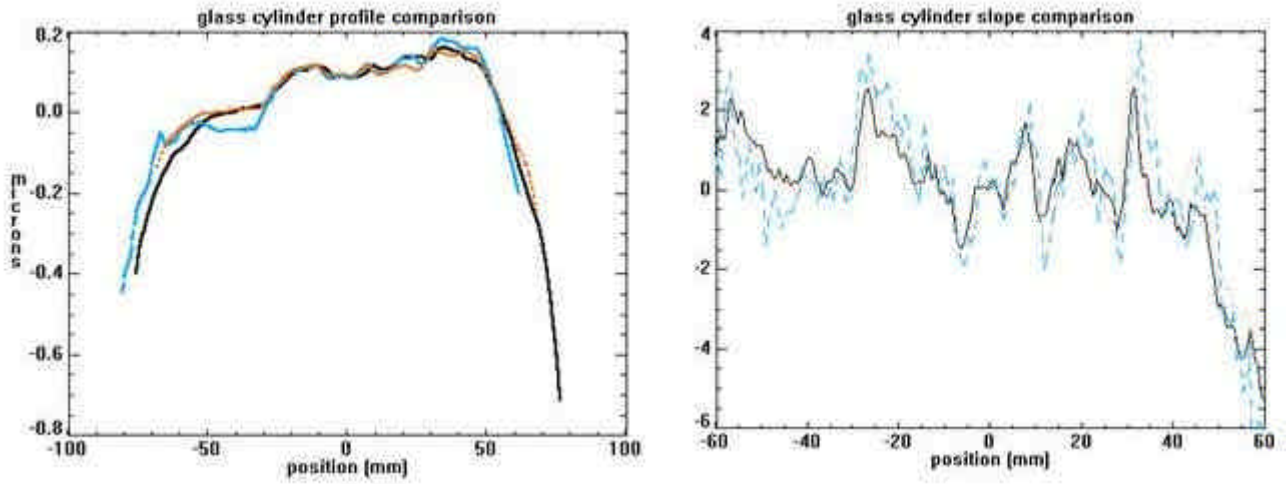

Fig.3: comparison of CGH interferometry, Long trace profilometry, and collimated beam interferometry on a glass cylinder; Left: axial figure profile, right: axial slope irregularity profile. Black: CGH-based interferometry; Dashed grey: collimated beam interferometry; dotted grey: LTP.

Fig. 4 shows the current implementation of this measurement. As there is no commercially available 20cm beam expander for commercial phase shifting interferometers, we built one in-house using a high quality (?/20 P/V @633nm) off-axis parabolic mirror on an optical rail. A set of movable, adjustable fold flats and various test fixtures allow redirection of the collimated beam depending on the measurement required:

a) "stand-alone" substrate or replica axial figure measurement in a custom (low shape perturbance) test fixture
b) mandrel axial figure measurement
c) "in-situ" measurement of an optic in a test alignment housing (Fig. 3 shows this configuration in particular).

Note that this test does NOT measure absolute slope. The local or global cone angle of the optic can change without changing the interferogram. The quantities determined are usually described as (1) axial curvature or sag, and (2) axial figure (or slope) irregularity. Typically in our analysis, and in the error budget, these two terms are separated. Figure 5 shows an example of this for a formed substrate (measured axially at five equally spaced azimuthal positions) and for the same optic after replication. The smooth curves are taken from axial measurements of the forming mandrel. The

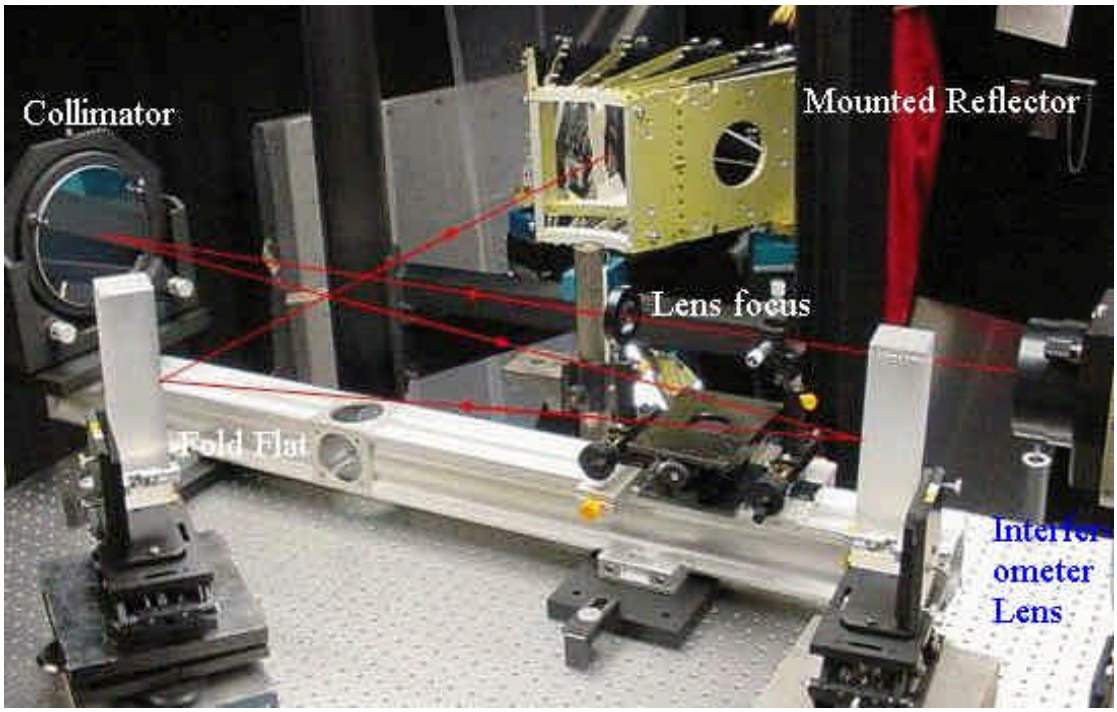

Fig. 4: Picture of the interferometry setup, positioned to direct the collimated beam into the housing to test axial figure of a test optic in-situ. The interferometer transmission sphere (far right) directs the beam through the spatial filter to the 20 cm off-axis parabolic collimator; the two 22.5 cm fold mirrors then redirect the beam through the system axis so as to be aligned normal to the test mirror surface.

curvature (expressed as a second order fit coefficient to a polynomial in the axial coordinate) and the optic figure error (from the mandrel) standard deviation are listed at the right and left edge of each trace respectively.

The data show that the forming process (see [5,6]) imparts significant high frequency figure error, but the overall shape conforms very well to the forming mandrel. The replication process corrects for this high frequency ripple. It is also

evident that the current forming mandrels do not have the required axial figure; we are working to correct this to improve the overall optic quality.

3.3.1 Axial profile repeatability

We have tested both short term repeatability and the ability to remeasure a given part after removing it and reinstalling it in the axial metrology station. The latter is important, as the replication process can induce small stresses which may relax over time. Again it is useful to distinguish sag measurement from figure or slope irregularity. Measurements on a small, axially sloped mandrel show a short term repeatability of 1 $\mu m/m^2$ as compared to an overall error budget allocation of 10 $\mu m/m^2$. Slope uncertainties, as examined both on mandrel measurements and substrate measurements, are of the order 0.35 arcsec (rms); this is somewhat surprising, as the substrates are much more prone to environmental errors, such as vibration. Figure 6 shows two repeat measurements of the local slope on a (smaller) replication mandrel we figured and polished for the C-X optics program (in this case for the hard x-ray telescope or HXT). All features significant for either the SXT or HXT (Hard x-ray telescope) figuring levels repeat, but at finer levels there are variations.

Another means of checking the response of the axial figure station is by measuring the same part with other, overlapping metrology capabilities. We performed a comparison of the axial interferometry, Bauer midfrequency, and two different magnifications of microroughness measurement was undertaken, using recently replicated mirrors for the OAP

development. Figure 7 shows the results, represented as estimates of the power spectral density. The Bauer and 2.5x microroughness data both overlap the axial interferometry to some extent, and the microroughness and Bauer data overlap as well. Overall the PSD is smoothly varying although the slope increases at spatial frequencies below ~2 mm^{-1} as we have observed before. This data is taken from a few scans on each instrument; as the optics improve we expect to study the best reflectors more thoroughly.

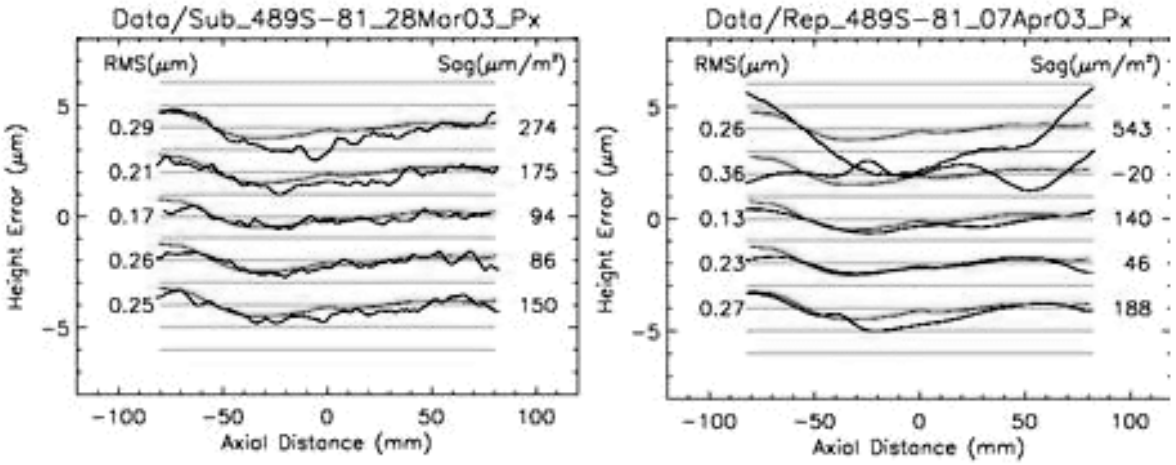

Fig. 5: Axial profiles at five azimuthal positions as compared to a forming mandrel (uniform superimposed curve) for a formed substrate (left) and the same part after replication from a high-accuracy replication mandrel (right). The axial sag coefficient (right edge) and the standard deviation of the differential figure from the forming mandrel (left edge) are listed next to each profile. Vertical offsets are for clarity, but the vertical scale is uniform

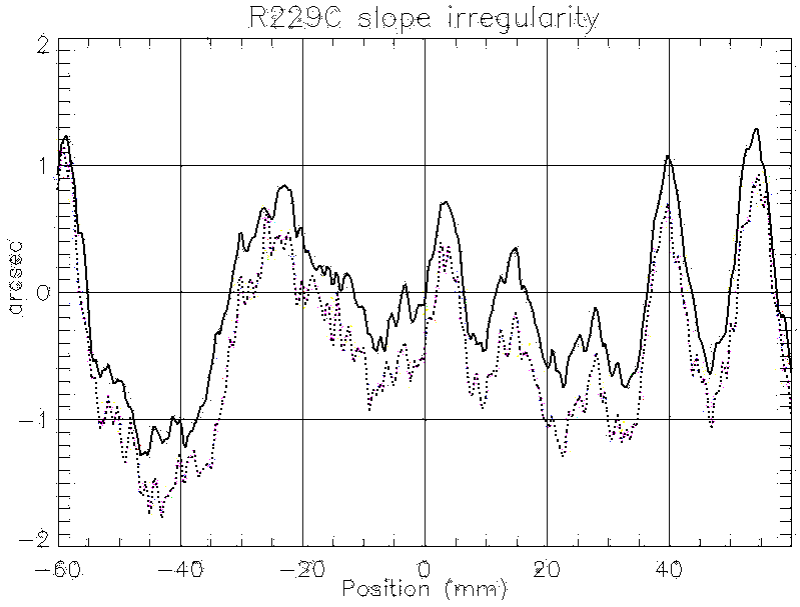

Fig. 6: Repeatability data on axial slope irregularity, as measured on a precision replication mandrel figured in-house at GSFC; offset of 0.5 arcsec is for clarity. The rms repeatability error is ~0.35 arsec.

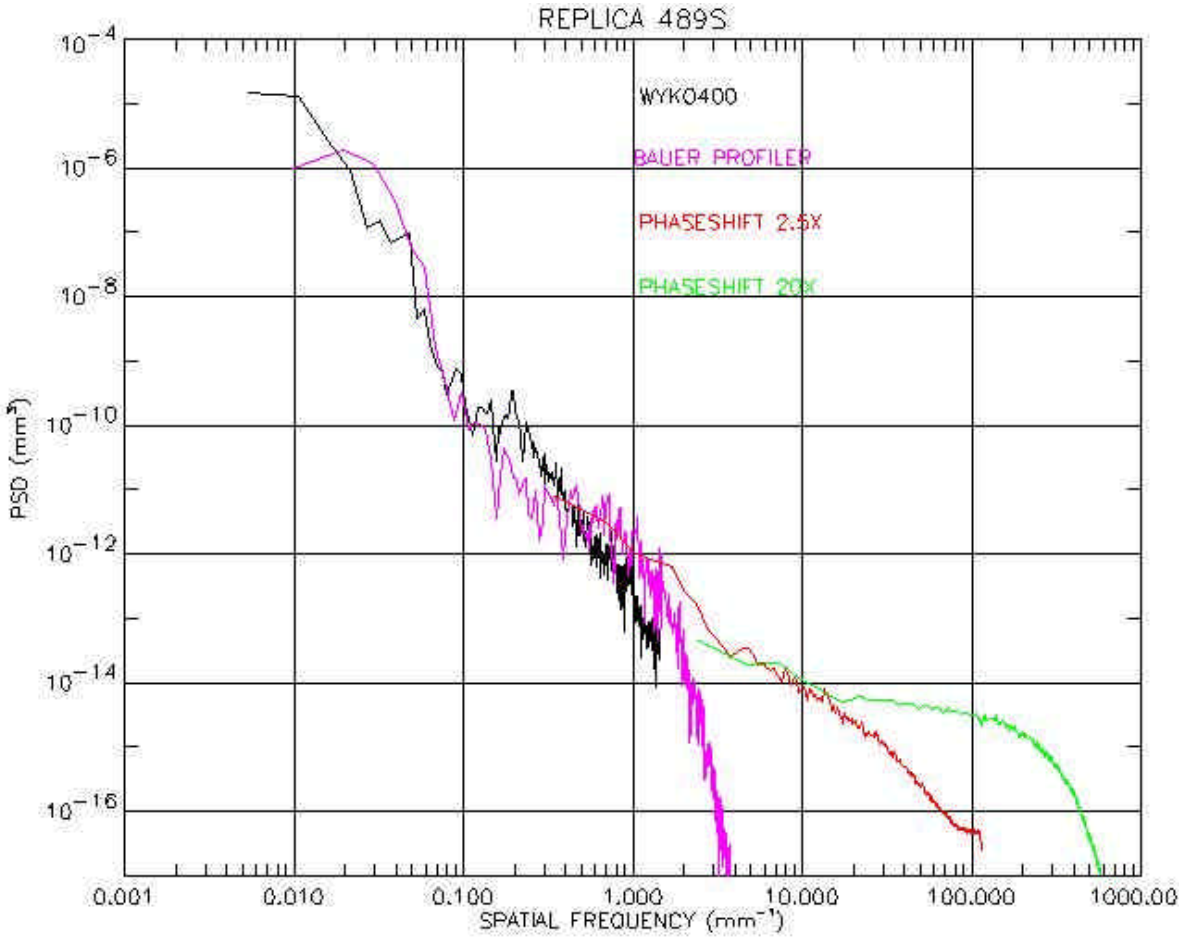

Fig. 7: Power spectral density for multiple measurements on replicas 489S-126 & S-127; from low to high spatial frequency these are axial figure, Bauer mid-frequency, 2.5x, and 20x microroughness; agreement in the overlap regions is good and the overall spectrum (except at the high frequency end of each measurement where the noise dominates) is smooth.

This is an indication that the dominant error in these optics continues to be low-order figure errors as noted above.

3.4 Midfrequency error

This error has not been a significant area requiring development to date on this program; the means of measurement is the Bauer200 [16], which measures local curvature very accurately. Typically the midfrequency error on replicated segments has not been measured to be excessive. In addition, we have observed good agreement between the Bauer data and the axial interferometry data for errors in the spatial frequency range down to ~ 1 mm.. Fig. 7 shows an example, in this case converted to a power spectrum, of the same replicated mirror as measured both with axial interferometry and with the Bauer200. We have also examined repeatability data and noise-equivalent power spectra to determine for each measurement where the signal-to-noise in the power spectrum falls off; typically these measurements need to be complemented by higher frequency measurements such as microroughness measurements at about an error period of 0.5mm.

3.5 Microroughness

This measurement is performed using a optical microinterferometer. We have reengineered one of these to be able to directly measure roughness on a forming mandrel (0.5m diameter by 0.3m axial length) which is much thicker than the standard 'tall parts' commercially available version. This setup is shown in Fig. 8. Recently we were able to compare roughness of a small test coupon we polished among our measurement and two roughness determinations made using x-ray scattering. Table 5 shows the close agreement, including overlapping error bars, among these three assessments of the same sample. This is true in spite of the fact that the three measurements each have a differing range of spatial frequencies (see, e.g, Bixler at al [17] for a discussion of spatial frequencies accessible to x-ray scattering methods). We take this as good evidence that our microroughness data is usable to an uncertainty of 0.05 nm rms.

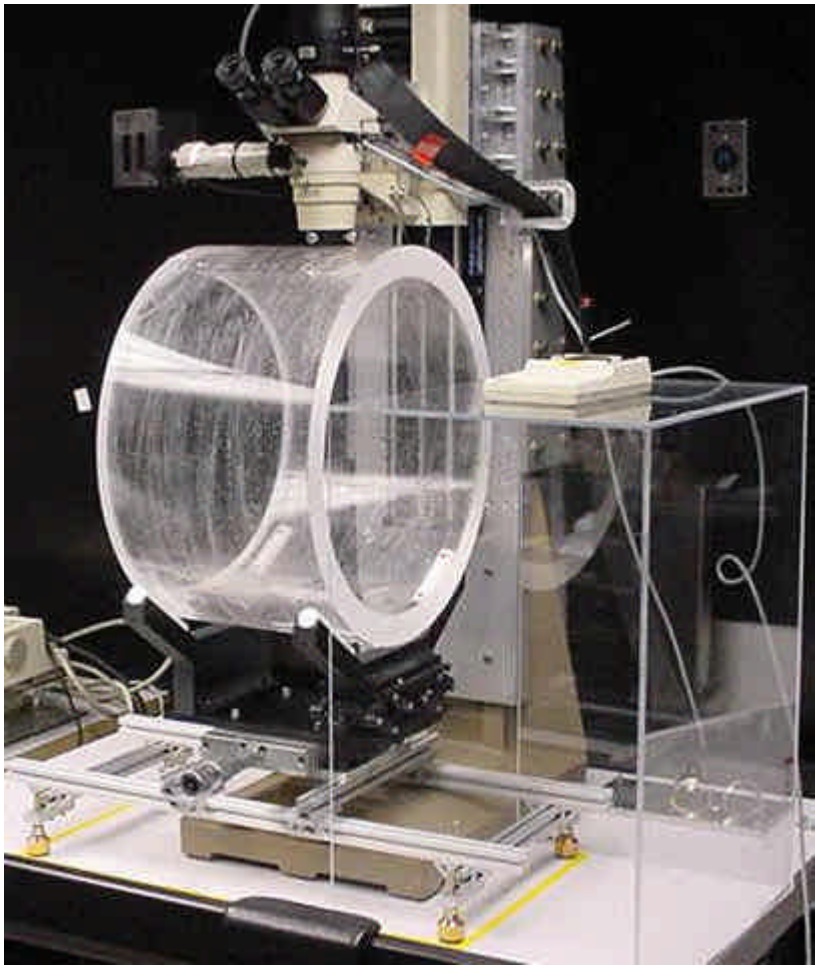

Fig. 8: Wyko TOPO-3D roughness microinterferometer, remounted to allow measurements of large mandrels. A 50 cm diameter, 30cm length forming mandrel is being measured for surface roughness.

Table 5: Roughness results on test coupon	**Roughness, nm rms**	
Type of test	average	stdev
F. Christensen/DSRI X-ray scatter	0.45	0.02
S. Owens, GSFC X-ray scatter	0.48	0.04
GSFC optical microinterferometry	0.40	0.08

4. SUMMARY

We summarize the motivation, requirements, and progress to date in optical metrology in support of the Constellation-X soft x-ray telescope technology development program. Mandrel shape as well as mandrel and reflector axial metrology are adequately performing and are well understood. Reflector shape measurements are still in an early state. We expect within the next year to demonstrate that metrology in all areas is well understood and adequately accurate and precise to support the flight tolerances for this challenging instrument.

5. ACKNOWLEDGEMENTS

This work was funded through the C-X technology development program; we acknowledge Dr. R. Petre, J. Grady, and D. Nguyen for their able management. Assistance in developing and operating various metrology stations was provided by T. Wallace, L. Kolos, C. Strojny, J. McMann, Dr. P. Arsenovic, T. Faulkner, T. Mengers, and L. Worrel. We acknowledge W. Egle, P. Glenn, B. Jones, P. Takacs, S. O'Dell for useful discussions on metrology on x-ray optics. The scatter measurements done using x-rays by Scott Owens and Finn Christensen are much appreciated. Mention of trade names or commercial products does not constitute endorsement or recommendation by the authors, NASA, Mantech, or Swales Aerospace.

6. REFERENCES

[1] See the description of Constellation-X online at http://constellation.gsfc.nasa.gov/

[2] R. Petre, "Recent progress on the Constellation-X spectroscopy x-ray telescope (SXT)," Proc. SPIE [**5168**-21] (2003).

[3] T. T. Saha, D. A. Content, W. W. Zhang , "Equal-curvature x-ray telescope designs for Constellation-X mission," Proc. SPIE [**5168**-37] (2003).

[4] W. A. Podgorski, J. Bookbinder, et al., "Constellation-X spectroscopy x-ray telescope image error budget and performance prediction," Proc. SPIE [**5168**-35] (2003).

[5] W. W. Zhang, K. Chan, D. A. Content, R. Petre, P. J. Serlemitsos, T. T. Saha, Y. Soong, "Development of mirror segments for the Constellation-X Observatory," Proc. SPIE **4851**-58 (2002).

[6] W. W. Zhang, "Development of mirror segments for the Constellation-X mission," Proc. SPIE [**5168**-19] (2003)..

[7] S. M. Owens, J. J. Hair, ; W. A. Podgorski, P. Glenn, J. Stewart, et al., "Constellation-X SXT optical alignment Pathfinder 2: design, implementation, and alignment, " Proc. SPIE [**5168**-27] (2003).

[8] S. L. O'Dell, M. A. Baker,.; D. A. Content, ; M. D. Freeman, P. Glenn, M. V. Gubarev, et al., "X-ray testing Constellation-X optics at MSFC's 100-m facility", Proc. SPIE [**5168**-34] (2003).

[9] T. Hadjimichael, D. Content, G. Wright, ; C. Fleetwood, D. Colella, et al., "Noncontact metrology on segmented x-ray optics for the Constellation-X SXT," Proc. SPIE [**5168**-24] (2003).

[10] T. Hadjimichael, D. A. Content, C. Fleetwood E. Waluschka, G. Wright, "Non-Contact Shape Measurements of Ultra-Lightweight X-Ray Optics," Proc. ASPE (2003).

[11] H. Wolter, "Mirror systems with glancing incidence on image producing optics for x-rays, " Ann. Phys. **10**, 94-114 (1952).

[12] P. Glenn, "Centroid detector assembly for the AXAF-I alignment test system," Proc. SPIE **2515**, 352 (1995).

[13] Microtrak 7000 Laser Displacement Sensor, MTI Instruments.

[14] S. Qian, J. Werner, P. Takacs, "The penta-prism LTP: A long-trace-profiler with stationary optical head and moving penta prism (abstract) Rev. Sci. Inst. **66** (2), 2187 (1995).

[15] M. V. Gubarev, T. Kester, P. Takacs, "Calibration of a vertical-scan long trace profiler at MSFC," SPIE 4451, 333-339 (2001).

[16] P. Glenn, "Robust Å level circularity profilometry," Proc. SPIE **1333**, 230-238 (1990).

[17] J. Bixler, C. Mauche, C. Hailey, L. Madison, "Reflectivity and scattering measurements on and Advanced X-ray Astrophysics Facility test coating sample, " Appl. Opt.**34** 6542-6551 (1995).